Elena I. Smotrova

DEVELOPMENT OF NYSTROM-TYPE TECHNIQUES FOR EFFICIENT COMPUTATION OF 2-D DIELECTRIC RESONATORS AND SCATTERERS

Home institution
Institute of Radiophysics and Electronics of the National Academy of Sciences of Ukraine
Akademika. Proskury str., 12
Kharkiv 61085, *Ukraine*
Tel: (+380) 57 7203782, *Fax*: (+380) 57 3152105
e-mail: elena.smotrova@gmail.com

Host Institution
Laboratoire de Photonique Quantique et Moleculaire, CNRS UMR 8537,
Ecole Nationale Superieur de Cachan,
Cachan 94235
France

Project duration : 6 month
Start date : 17 April 2012 End date : 17 October 2012

PUBLICATIONS RELATED TO PROJECT

with acknowledgement to ESF RNP Newfocus

1. M.V. Balaban, E.I. Smotrova, O.V. Shapoval, V.S. Bulygin, A.I. Nosich, "Nystrom-type techniques for solving electromagnetics integral equations with smooth and singular kernels," *Int. J. of Numerical Modeling: Electronic Networks, Devices and Fields*, vol. 25, no 5, pp. 490-511, 2012.

2. E.I. Smotrova, V. Tsvirkun, I. Gozhyk, C. Lafargue, C. Ulysse, M. Lebental, A.I. Nosich, "Spectra, thresholds and modal fields of a kite-shaped microcavity laser: analysis with Muller integral equations and Nystrom method," *J. Optical Society of America B,* 2012 (will be submitted shortly).

3. E.I. Smotrova, R. Sauleau, A.I. Nosich, "Near and far fields of a kite-shaped dielectric resonator antenna," *Proc. European Conf. Antennas and Propagation (EuCAP-2012)*, Prague, 2012, A07-3.3.

4. E.I. Smotrova, I. Gozhyk, M. Lebental, A.I. Nosich, "Accurate modeling of microcavity lasers with symmetry lines based on Muller's integral equations," *Proc. Int. Conf. Near-Field Optics (NFO-12)*, San Sebastian, 2012.

5. E.I. Smotrova, "Linear optical modeling of microcavity laser modes: thresholds, frequencies, directivities" (Invited Paper), *Proc. Int. Conf. Mathematical Methods in Electromagnetic Theory (MMET*12)*, Kharkiv, 2012, pp. 29-34.

6. E.I. Smotrova, I. Gozhyk, M. Lebental, A.I. Nosich, "Studying the microcavity lasers as active dielectric resonator antennas," *Proc. Int. Symp. Antennas and Propagation (ISAP-2012)*, Nagoya, 2012, pp. 967-970.

SCIENTIFIC REPORT

Summary

In this project we have considered the simulation of 2-D dielectric resonators in free space using the Muller Boundary integral equations (BIE). We have developed interpolation-type Nystrom method of the BIE reduction to the discrete form that has theoretically proven convergence. Here, convergence is understood in mathematical sense, as a possibility of progressive minimization of the error of computations by taking the greater orders of interpolation scheme. Implementing the developed algorithm we have performed a systematic numerical analysis of the natural frequencies

and also the near and far-zone fields for the natural modes of the dielectric-resonator shaped as a kite with the contour changing from fully convex to partially concave. The influence of the deviation from the circular shape on the modal characteristics has been studied numerically, demonstrating the opportunities of improvement of directionality of the far-field emission. Comparison with experimental measurements made in Cachan for large-size dielectric resonators used in microlasers has shown qualitative agreement in far-field radiation patterns.

Motivation and goal

Dielectric resonators are ubiquitous building blocks of various electromagnetic-wave systems across a wide spectrum of frequencies, from millimetre waves to the visible range, and applications. This is explained, in part, by the availability of modern low-loss materials and also by the fact that the metals become prohibitively lossy at higher frequencies. One of the most important applications of dielectric resonators is in the design of antennas, where the high Q-factor of a resonating mode enables one to raise the radiation resistance (i.e. the power at the fixed current) of primary feed. Another important application is the design of laser sources of the terahertz, infrared and visible ranges: in this case the main part of the device is a semiconductor cavity, which can be conveniently considered as a dielectric resonator equipped with an active region. Because of intrinsic necessity of radiation into outer space, any such laser can be viewed as an active dielectric resonator antenna.

On the other hand, many other electromagnetic devices with different operation principles may, unwillingly for the designer, display their resonant properties if made of dielectric. As an example of this effect one can find in the spoiling of the focusing ability of a finite-size dielectric lens if the wavelength comes near to one of the natural-mode wavelength. All mentioned makes the task of accurate analysis of dielectric resonators a hot topic in today's electromagnetic theory. This is, however, a complicated task as analytical solutions can be built only for separable configurations such as circular cylinders and spheres. Still many resonators are shaped as thin flat structures. In this case one can reduce the dimensionality of the problem from 3-D to 2-D however the bulk dielectric permittivity has to be replaced with its (frequency dependent) effective value and the electromagnetic field is considered in the resonator median plane only.

Therefore my goal during the "Newfocus" exchange-grant stay in Cachan has been the development of several novel and efficient numerical techniques for the computation of natural modes of 2-D dielectric resonators of arbitrary shape. The same techniques are equally applicable to the analysis of the wave scattering by corresponding configurations.

Background

As known, dielectric resonators shaped as thin flat circular disks with smooth enough rims demonstrate very high Q-factors however very low directionality of the whispering-gallery modes [1-4]. Here, each mode with azimuth index $m > 0$ is double degenerate and their emission is predominantly in the dielectric resonator plane. The directivity is equal to 2 because of many identical beams corresponding to the $\cos m\varphi$ or $\sin m\varphi$ dependence (φ being the azimuth coordinate). In practical applications, however, it is required to have dielectric resonator antennas with larger directivity of emission to enable processing of signals with higher efficiency and within smaller space.

As evident, improvement of directionality of mode emission needs a departure from circular shape. Therefore since the 1990s researchers engaged in the dielectric resonator studies have been using the cavity shape as an engineering tool able to provide better directionality [5-24]. Among the promising modified shapes, they have considered fully convex contours like ellipse, stadium, cut circle, various regular polygons, and others [9-13], and also partially concave "notched" contours" [14,15]. Probably the highest expectations and the largest amount of efforts have been associated with a spiral resonator, whose in-plane contour follows an Archimedean spiral with a small step [17-21]. The later efforts have been associated with a smoother shape provided by the limacon curve [22-24]. Following similar considerations, it is possible to find other smooth perturbations of the circle; one of them being a curve called "kite" that we have selected for a detail analysis. Unlike a limacon, a kite is always smooth although it can be both fully convex and partially concave depending on the perturbation parameter.

In this work, we have used the Muller boundary integral equations (BIEs) [25,26] as a reliable and efficient tool for the analysis of electromagnetic field in the presence of a 2-D homogeneous

dielectric object with arbitrary smooth boundary. This is because other types of BIEs suffer of serious drawback: they possess infinite number of "spurious eigenvalues" – real numbers that are the eigenvalues of the interior electromagnetic problem where the boundary is assumed perfectly electrically conducting and the inside filling has material parameters of the outer medium (e.g., free space) [27]. The spurious eigenvalues have no physical meaning and hinder the search of true complex eigenvalues. Examples of such IEs can be found in [10,15,18,19,21,23,24]; it should be added that these IEs can be still used for the search of low-Q eigenvalues.

In 2-D, Muller BIE is, in fact, two coupled equations. Besides of being free of spurious eigenvalues, they are attractive because they are of the Fredholm second-kind type, i.e. have smooth or integrable kernels. The Muller BIEs can be discretized either with collocations [28] (i.e., meshing the boundary and introducing local basis functions; this is sometimes called the boundary-element method, BEM) or with a Galerkin-type projection to global expansion functions [26]. As dielectric resonators commonly have convex or at least star-like boundaries, the latter way leads to a more economic algorithm, although the both possess a convergence thanks to the Fredholm theorems. Within the "Newfocus" project I have been building efficient and convergent numerical algorithm based on the interpolation polynomials and the quadrature formulas as suggested in [29,30].

Formulation

We denote the smooth boundary of a generic 2-D open dielectric resonator as Γ, the outer domain as D_e, and the inner domain as D_i. We assume that $\vec{n}$ is the outer normal unit vector to the boundary Γ, and ν_j ($j = i, e$) are the refractive indices of the non-magnetic resonator material and the outer space, respectively. The time dependence $\exp(-i\omega t)$ will be assumed and omitted. The inner domain is filled with dielectric material so that the associated refractive index is ν_i. The outer space is assumed lossless, $\nu_e = \alpha_e > 0$.

The passive dielectric cavities ($\mathrm{Im}\,\nu_i \geq 0$) are known to possess infinite number of discrete complex-valued natural frequencies or, equivalently, wavenumbers k_s ($\mathrm{Im}\,k_s < 0$), each of which generates the corresponding non-zero electromagnetic field function, $\{\vec{E}_s, \vec{H}_s\}$. The field functions grow in space as $O(e^{-\mathrm{Im} k_s R})$. Therefore, to avoid dealing with complex k_s and non-physically growth of the field functions, we will assume that the dielectric resonator is filled in with a gain material, i.e. is active. This can be characterized using the complex-valued refractive index, $\nu_i = \alpha_i - i\gamma$ where $\gamma > 0$. The presence of the gain region (here coinciding with the whole dielectric-resonator domain) enables compensation for the radiation losses of any specific mode and makes its natural wavenumber k_s real-valued. The associated value of $\gamma_s > 0$ is generally different for different modes and corresponds to the threshold gain in the resonator material [31].

Mathematically, the problem of finding the values of k_s and γ_s, and also the modal fields $\{\vec{E}_s, \vec{H}_s\}$ in the near and far zones makes an electromagnetic eigenvalue problem (similar to the scattering problem but without the incident field). In view of the 2-D cavity studied here, to characterize the electromagnetic field we can consider a scalar function U_j that is the field component E_z or H_z, depending on the polarization, in the domains D_j, $j = i, e$. It must be a solution to the boundary-value problem for the Helmholtz equations with the continuous boundary conditions on Γ, and additional conditions of (i) local power finiteness and (ii) outgoing-wave behavior (Sommerfeld radiation condition) for U_e at infinity [3, 26]. The task is to find such values of pairs of real numbers (k_s, γ_s) that generate non-zero functions $U_{i,e}(\vec{r})$. Note that the real value of k_s means that the natural mode at the threshold of lasing does not attenuate in time and decays in space as a usual cylindrical wave, $\sim O(r^{-1/2})$. Thus, the introduction of the active region into a dielectric resonator leads to physically reasonable modal field behavior.

Basic equations

For either of two alternative polarizations, the reduction of the 2-D electromagnetic-filed eigenvalue problem to a BIE is based on the use of the Green's formulas [25,29]. Then from the boundary conditions we obtain

$$\varphi(\vec{r})+\int_{\Gamma}\varphi(\vec{r}')A(\vec{r},\vec{r}')dl'-\int_{\Gamma}\psi(\vec{r}')B(\vec{r},\vec{r}')dl'=0\,. \tag{1}$$

$$\frac{\eta_i+\eta_e}{2\eta_e}\psi(\vec{r})+\int_{\Gamma}\varphi(\vec{r}')C(\vec{r},\vec{r}')dl'-\int_{\Gamma}\psi(\vec{r}')D(\vec{r},\vec{r}')dl'=0\,, \tag{2}$$

where $\varphi(\vec{r})=U_i(\vec{r})$ and $\psi(\vec{r})=\dfrac{\partial U_i(\vec{r})}{\partial n}$. Equations (1) and (2) form the set of the Muller boundary integral equations. Here, the kernel functions are

$$A(\vec{r},\vec{r}')=\frac{\partial G_i(\vec{r},\vec{r}')}{\partial n'}-\frac{\partial G_e(\vec{r},\vec{r}')}{\partial n'},\ B(\vec{r},\vec{r}')=G_i(\vec{r},\vec{r}')-\frac{\eta_i}{\eta_e}G_e(\vec{r},\vec{r}')\,, \tag{3}$$

$$C(\vec{r},\vec{r}')=\frac{\partial^2 G_i(\vec{r},\vec{r}')}{\partial n\partial n'}-\frac{\partial^2 G_e(\vec{r},\vec{r}')}{\partial n\partial n'},\ D(\vec{r},\vec{r}')=\frac{\partial G_i(\vec{r},\vec{r}')}{\partial n}-\frac{\eta_i}{\eta_e}\frac{\partial G_e(\vec{r},\vec{r}')}{\partial n},$$

The Green's function of a homogeneous medium having refractive index ν_i is $G_j(\vec{r},\vec{r}')=(i/4)H_0^{(1)}(k_jR)$, where $R=\left|\vec{r}-\vec{r}'\right|$ is the distance between the points $\vec{r}$ and $\vec{r}'$, and $H_0^{(1)}(\cdot)$ is the Hankel function of the first kind and zero order. We defined that $k_{i,e}=k\nu_{i,e}$, the constants $\eta_{i,e}=1/\nu_{i,e}^2$ in the case of the H -polarization and $\eta_{i,e}=1$ in the case of the E-polarization. The normal derivatives are calculated after the following expressions:

$$\frac{\partial G_j(\vec{r},\vec{r}')}{\partial n'}=(i/4)k_jH_1^{(1)}(k_jR)(\vec{R}\cdot\vec{n}')/R,\quad \frac{\partial G_j(\vec{r},\vec{r}')}{\partial n}=(-i/4)k_jH_1^{(1)}(k_jR)(\vec{R}\cdot\vec{n})/R \tag{4}$$

$$\frac{\partial^2 G_j(\vec{r},\vec{r}')}{\partial n\partial n'}=-\frac{ik_j}{4}\left[k_jH_2^{(1)}(k_jR)(\vec{R}\cdot\vec{n}')\frac{(\vec{R}\cdot\vec{n})}{R^2}-H_1^{(1)}(k_jR)\frac{(\vec{n}'\cdot\vec{n})}{R}\right]$$

The quantities $(\vec{R}\cdot\vec{n})$, $(\vec{R}\cdot\vec{n}')$ and $(\vec{n}'\cdot\vec{n})$ are the scalar products of the corresponding vectors.

Thus, the kernels of the Muller BIE are the linear combinations of either the Green's functions of the homogeneous media having parameters of the outer and inner media, or their normal derivatives of the first and second order. Assuming that the contour parameterization is performed with the aid of the function $r(t)=\{x(t),y(t)\}$, we find that the kernel functions $A(t,\tau)$ in and $D(t,\tau)$ in are continuous at all points of a smooth contour, and the kernel functions $B(t,\tau)$ and $C(t,\tau)$ have logarithmic singularities. Note that the kernel $B(t,\tau)$ is singular only in the case of the H-polarization; in the case of the E-polarization it is continuous.

As mentioned, there are several ways of reasonable discretization of BIEs. One of the most efficient discretization techniques is the method of quadratures also known as Nystrom method [29,30,32-34]. This method is based on the approximation of smooth unknown functions by certain polynomials and the replacement of the integrals with approximate sums using the appropriate quadrature formulas. Therefore the center point in the development of corresponding numerical algorithms is placed on the derivation of the quadrature formulas that correctly take into account the behavior of the integrand functions and first of all their possible singularities.

We consider the discretization of integral equations with closed contours of integration that admit a regular analytical 2π-periodic parameterization with the aid of a function $\mathrm{r}(t)=\{x(t),y(t)\}$, $t\in[0,2\pi]$. As some of the kernel functions have logarithmic singularities, it is convenient to represent all of them in such a way that these singularities are extracted; such decomposition is done for the smooth kernels as well

$$F(t,\tau)=F_1(t,\tau)\ln\left[4\sin^2\frac{t-\tau}{2}\right]+F_2(t,\tau),\quad F=A,B,C,D\,, \tag{5}$$

where $A_1(t,\tau), B_1(t,\tau), C_1(t,\tau)$ and $D_1(t,\tau)$ are the analytic functions defined as follows:

$$\begin{aligned}
&A_1(t,\tau) = (-1/4\pi)\left[k_i J_1(k_i R) - k_e J_1(k_e R)\right](\vec{R}\cdot\vec{n}')/R,\\
&B_1(t,\tau) = (-1/4\pi)\left[J_0(k_i R) - (\eta_i/\eta_e) J_0(k_e R)\right],\\
&C_1(t,\tau) = (1/4\pi)\left[k_i^2 J_2(k_i R) - k_e^2 J_2(k_e R)\right](\vec{R}\cdot\vec{n}')(\vec{R}\cdot\vec{n})/R^2 - \\
&\qquad\qquad (1/4\pi)\left[k_i J_1(k_i R) - k_e J_1(k_e R)\right](\vec{n}'\cdot\vec{n})/R,\\
&D_1(t,\tau) = (1/4\pi)\left[k_i J_1(k_i R) - (\eta_i/\eta_e) k_e J_1(k_e R)\right](\vec{R}\cdot\vec{n})/R
\end{aligned} \tag{6}$$

The functions $A_2(t,\tau), B_2(t,\tau), C_2(t,\tau), D_2(t,\tau)$ are found from (5) with account of (3)-(4). Further, we introduce an equidistant mesh of nods on the contour Γ at $t_p = \pi p/N$, $p = 0,1,...,2N-1$. The integrals of the each part of kernels are replaced with the sums using the quadrature formulas. For the logarithmic parts we use the quadrature formula derived through the approximation of the integrand function with trigonometric polynomials [29,30,32-34],

$$\int_0^{2\pi} \ln\left[4\sin^2\frac{t-\tau}{2}\right] F_1(t,\tau) f(\tau) L(\tau) d\tau \approx \sum_{p=0}^{2N-1} P_p^{(N)}(t) F_1(t,t_p) f(t_p) L(t_p), \tag{7}$$

where the $P_p^{(N)}(t) = -(2\pi/N)\sum_{m=1}^{N-1}\cos\left[m(t-t_p)\right]/m - \pi\cos\left[N(t-t_p)\right]/N^2$ is a trigonometric polynomial. For the other, continuous parts of kernels we use the trapezoidal rule ([35]). In the formulas (7) it is implied that $F_1 = A_1, B_1, C_1, D_1$, and also $f = \varphi, \psi$. The function $L(t)$ is the Jacobian.

On the replacement, in the integral equations (1) and (2), of the integrals with the quadratures we arrive at the following matrix equation of the size $4N \times 4N$

$$\left[\mathbf{I} + \mathbf{A}\right](\Phi, \Psi) = 0, \tag{8}$$

where the vectors of unknowns are $\Phi = \left\{\varphi(t_p)\right\}_{p=0,2N-1}$ and $\Psi = \left\{\psi(t_p)\right\}_{p=0,2N-1}$, and the matrix $\mathbf{A}$ has a block structure,

$$\mathbf{A} = \begin{bmatrix} A & -B \\ C & -D \end{bmatrix} \tag{9}$$

Every block has the size of $2N \times 2N$ and its elements are given by

$$\begin{aligned}
&A = \left\{(P_p^{(N)}(t_s) A_1(t_s,t_p) + (\pi/N) A_2(t_s,t_p)) L(t_p)\right\}_{p,s=0}^{2N-1},\\
&B = \left\{2\eta_e/(\eta_e+\eta_i)(P_p^{(N)}(t_s) B_1(t_s,t_p) + (\pi/N) B_2(t_s,t_p)) L(t_p)\right\}_{p,s=0}^{2N-1},\\
&C = \left\{(P_p^{(N)}(t_s) C_1(t_s,t_p) + (\pi/N) C_2(t_s,t_p)) L(t_p)\right\}_{p,s=0}^{2N-1},\\
&D = \left\{2\eta_e/(\eta_e+\eta_i)(P_p^{(N)}(t_s) D_1(t_s,t_p) + (\pi/N) D_2(t_s,t_p)) L(t_p)\right\}_{p,s=0}^{2N-1}
\end{aligned} \tag{10}$$

It is convenient to introduce dimensionless value of $\kappa = ka$ where a is some characteristic dimension of the 2-D dielectric-resonator. Then, the eigenvalues (κ, γ) are the roots of determinantal equation $\det\left[\mathbf{I} + \mathbf{A}(k,\gamma)\right] = 0$.

Considering the accuracy of computations, we can note that if the integrand function is analytic and 2π-periodic, then, according to [29], the error of interpolation has the order of $O[\exp(-\sigma N)]$, where $2N$ is the number of nods in the quadrature and σ is the half-width of the strip in

the complex plane to which the integrand functions $F_{1,2}(t,\tau)f(\tau)L(\tau)$ can be continued holomorphically.

Further we present the numerical study of the H-polarized lasing modes of a 2-D dielectric-resonator shaped as a kite, Here, we can consider the cavity contour as a deformed circle and therefore study, in fact, the effect of the perturbation of the circle on the spectrum of frequencies and thresholds (or Q-factors) and also on the directionality of the emission. As a kite-contour parameterization, we use 2π-periodic analytical functions

$$x(t) = a(\cos t + \delta \cos 2t - \delta), \quad y(t) = a \sin t\,, \tag{11}$$

where a is the radius of a circular cavity in the limiting case of $\delta = 0$; we have studied in detail the cases of a fully convex contour for $\delta = 0.165$ and a partially concave contour for $\delta = 0.5$.

In Figs. 1 (a) and (b), we present the dynamics of the modal frequencies and thresholds in the kite dielectric resonator with varying deformation. Here, the curves for two pairs of modes are presented. One originates from two degenerated at $\delta = 0$ dipole modes of the $H_{1,4}$ type that have no whispering-gallery (WG) behavior. The other is related to two degenerated at $\delta = 0$ modes of the $H_{10,1}$ type that are clearly WG modes - to emphasize this, we will denote them as quasi-$WGH_{10,1}$. So far as the deformation is small, at least if $\delta < 0.15$, all four modes display similar behavior and actually WG-like modes are nearly degenerated while the non-WG modes become essentially split only in terms of the frequency. More dramatic changes happen if δ is getting larger end especially around and after the critical value of 0.251 where the kite obtains a concave part of the boundary. Each mode keeps its field function parity across the x-axis however its field pattern varies considerably. Note that the theorems of operator-valued function analysis guarantee that each $k_s(\delta)$ and $\gamma_s(\delta)$ are continuous functions of the argument. We label the corresponding continuous modal branches as I, II, III, and IV.

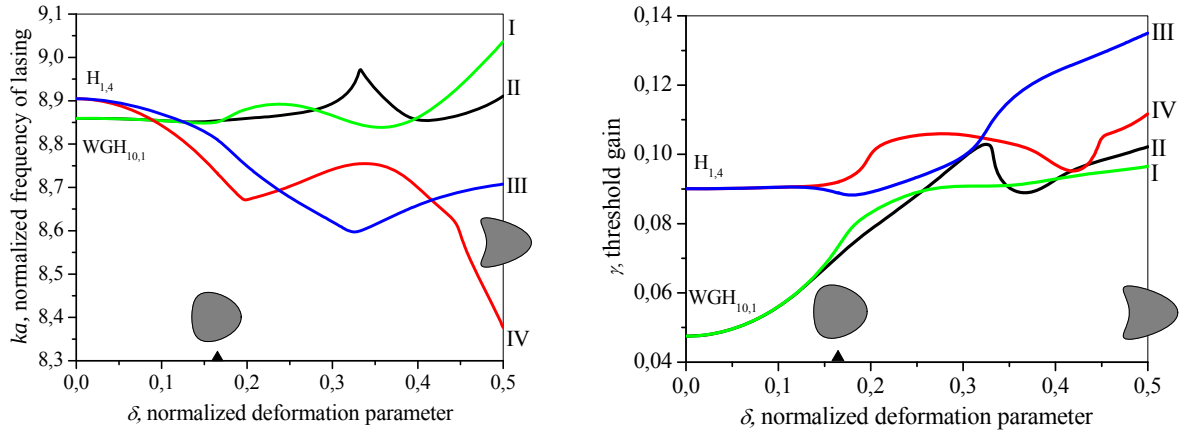

(a) (b)

Fig. 1. Frequencies (a) and thresholds (b) as functions of the kite deformation parameter δ, for the doublet of quasi-$WGH_{10,1}$ (green and black lines) and quasi-$H_{1,4}$ (blue and red) modes, $\alpha = 1.5$, $N = 50$. Marks I to IV correspond to similar marks in Fig. 2 and 3.

Figs. 2 and 3 demonstrate the amplitude near-field and far-field patterns for the doublets of modes $H_{1,4}$ and $WGH_{10,1}$ in a little-deformed convex kite-shaped dielectric-resonator and their eventual counterparts for the large deformation, respectively. The labels I to IV correspond to the marks in Figs. 1 (a) and (b). These field patterns enable one to see how the progressive deformation turns some of the initially WG-like modes into the Fabry-Perot (FP) like and volume modes. In addition, the field patterns of the mode in Fig. 4 demonstrate that in a strongly deformed kite cavity a specific family of modes appears which adapt themselves to the appearance of concave part of the boundary. We have called them “horse shoe-like” (HS-like) modes; they can be viewed, from the one hand, as a partial WG-like mode standing along the part of the dielectric-resonator boundary that is

still concave and, from the other hand, as a specific FP-like mode standing along the curved path between two most curved parts of the same boundary. HS-like modes also have rather low thresholds and radiate predominantly into the halfspace where the concave part of the contour is looking to.

Far-field expression for the mode field can be obtained using the asymptotic of the Hankel function for the large argument. This leads to the following formula:

$$U_e(r,\theta) \underset{r\to\infty}{=} -\frac{i+1}{4\sqrt{\pi k_e r}} e^{ik_e r}\Phi(\theta), \tag{12}$$

where θ is the angle of observation and $\Phi(\theta)$ is the far-field angular pattern,

$$\Phi(\theta) = \int_\Gamma \left\{ i\varphi k_e \left[\vec{n}'\cdot(\cos\theta,\sin\theta)\right] + \frac{\eta_i}{\eta_e}\psi \right\} e^{-ik_e[\vec{r}'\cdot(\cos\theta,\sin\theta)]} dl' \tag{13}$$

The directionality of mode emission can be conveniently characterized using the quantity borrowed from the antenna theory and called *directivity*,

$$D = \frac{2\pi}{P}|\Phi(\theta_{\max})|^2, \quad P = \int_0^{2\pi} |\Phi(\theta)|^2 \, d\theta, \tag{14}$$

where $\theta_{\max}$ is the angle of the main beam radiation in the halfspace $0 \le \theta \le \pi$ and P is, within a constant, the total power radiated by a lasing mode.

The values of directivity associated with each mode are also indicated in Figs. 2, 3 and 4. Note that all modes of a circular resonator with azimuth index $m > 1$ and far-field patterns $\Phi(\theta) = \cos m\theta$ or $\sin m\theta$ have $D = 2$ and that omni-directional emission for $m = 0$ results in $D = 1$. Note also that an x-odd mode cannot have less than two main beams and thus it displays generally (although not always) smaller values of directivity than its sister-mode of the x-even parity. As visible, the directivity of any mode of the kite cavity is larger than for the unperturbed WG mode of the circle.

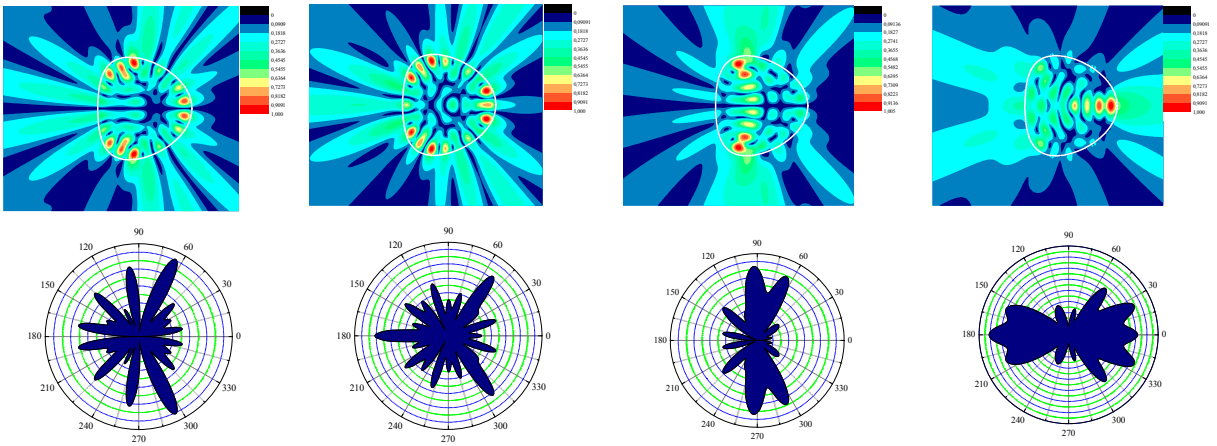

Fig. 2. Near- and far–field patterns of $|H_z|$ for two modes that form the quasi-$WGH_{10,1}$ doublet (I), (II) and quasi-$H_{1,4}$ doublet (III), (IV) in a kite with $\delta = 0.165$. These patterns correspond to the marks in Figs. 1. Mode (I) is an odd WG-like one with κ=8.8511, $\gamma = 7.352*10^{-2}$, $D = 3.86$. Mode (II) is an even WG-like one with $\kappa = 8.8534$, $\gamma = 7.076*10^{-2}$, $D = 3.33$. Mode (III) is an odd FP-like one with $\kappa = 8.8105$, $\gamma = 8.884*10^{-2}$, $D = 3.54$. Mode (IV) is an even FP-like one with $\kappa = 8.733$, $\gamma = 9.207*10^{-2}$, $D = 2.8$. Other parameters are $N = 50$, $\alpha = 1.5$.

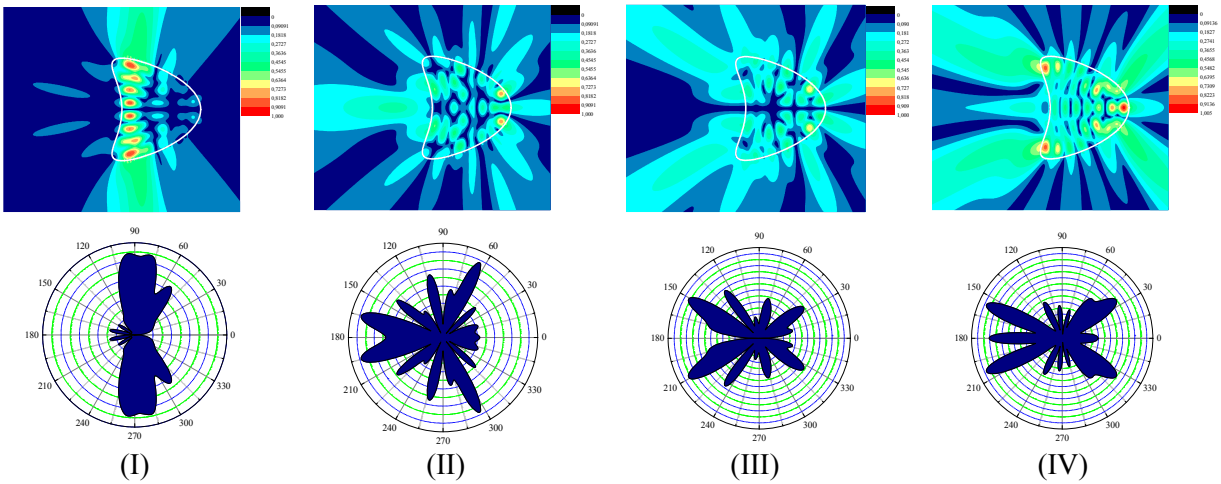

Fig. 3. The same as in Fig. 2 in a kite with contour parameter $\delta = 0.5$. These field patterns correspond to marks in Figs. 1. Mode (I) is an odd FP-like one with $\kappa = 9.0367$, $\gamma = 9.655*10^{-2}$, $D = 3.49$. Mode (II) is an even FP-like one with $\kappa = 8.9111$, $\gamma = 0.1022$, $D = 3.23$. Mode (III) is an odd volume one with $\kappa = 8.7076$, $\gamma = 0.135$, $D = 4.08$. Mode (IV) is an even volume one with $\kappa = 8.3764$, $\gamma = 0.1117$, $D = 3.95$.

Fig. 4. The same as in Fig. 3. Horse-shoe like mode is an odd one with $\kappa = 9.0652$, $\gamma = 8.1136*10^{-2}$, $D = 5.65$. Other parameters are $N = 50$, $\alpha = 1.5$.

Conclusions

In this project we have considered 2-D model of the uniformly active dielectric resonator with a smooth contour. As an instrument of analysis, we have used the Muller BIE adapted to the extraction of the lasing spectra and thresholds via the LEP formulation. We have also developed interpolation-type Nystrom method of the BIE reduction to the determinantal equation that has theoretically proven convergence. Here, convergence is understood in mathematical sense, as a possibility of progressive minimization of the error of computations (hence limited only by the machine precision) by taking the greater orders of interpolation scheme. Implementing the developed algorithm we have performed a systematic numerical analysis of the natural frequencies and thresholds, and also the near and far-zone fields for the modes of the dielectric-resonator shaped as a kite with deformation parameter changing the smooth contour from fully convex to partially concave.

In the kite resonator, the deformation of the contour from the circle leads to removal of the mode degeneracy and appearance of doublets. The kite-cavity modes that are the perturbations of the WG modes whose fields have been confined at the rim of the resonator are perturbed by the deformation in such a way that the thresholds of the both modes in a doublet monotonically grow up if the parameter δ gets larger. However they still keep relatively low values close to their (exponentially small) circular-cavity thresholds if the peak curvature of the kite contour remains close to unperturbed value. The critical value of the deformation parameter is $\delta \approx 0.251$ where the contour becomes partially concave. For the values of δ approaching 0.2 and larger, there are no modes whose fields display WG-like behavior along the whole boundary – all of them turn either to the FP-like modes or the other volume modes whose field spots are formed deep inside the kite cavity although HS-like modes show a string of brighter spots along the convex part of the boundary. The material thresholds of all modes of a concave kite are around the level of $\gamma \approx 0.1$ typical for the non-WG modes.

The directivities of the WG-like modes in a fully convex kite deformed with $\delta < 0.2$ can increase to 6-7 and show formation of a few well-shaped main beams of emission in the far zone.

The comparison of the measured spectral compositions of kite-shaped dielectric-resonators for microlasers and their far-field patterns with the computed spectra and patterns has enabled us to clearly identify the FP-like and the WG-like modes in both cases. The measured emission patterns and the computed ones show good qualitative agreement both in the directions of most intensive radiation and the "shining" parts of the cavity contour. The measured values of the lasing thresholds have displayed the expected difference between the WG-like modes and the FP-like ones, the latter being considerably higher than the former.

REFERENCES

1. S.L. McCall, A.F.J. Levi, R.E. Slusher, S.J. Pearton, and R.A. Logan, "Whispering-gallery mode microdisk lasers," Appl. Phys. Lett., **60** (3), 289–29 (1992).
2. A.B. Matsko and V.S. Ilchenko, "Optical resonators with whispering-gallery modes, Pt. 1, Basics and Pt. 2, Applications," IEEE J. Selected Topics Quantum Electronics, **12** (1), 3-32 (2006).
3. E.I. Smotrova, A.I. Nosich, T. Benson, and P. Sewell, "Cold-cavity thresholds of microdisks with uniform and non-uniform gain: quasi-3D modeling with accurate 2D analysis," IEEE J. Selected Topics Quantum Electronics, **11** (5), 1135-1142 (2005).
4. E.I. Smotrova, J. Ctyroky, T.M. Benson, P. Sewell, and A.I. Nosich, "Lasing frequencies and thresholds of the dipole-type supermodes in an active microdisk concentrically coupled with a passive microring," J. Opt. Soc. Am. A, **25** (11), 2884-2892 (2008).
5. A.F.J. Levi, R.E. Slusher, S.L. McCall, J.L. Glass, S.J. Pearton, and R.A. Logan, "Directional light coupling from microdisk lasers," Appl. Phys. Lett. **62** (6), 561-563 (1993).
6. H.G.L. Schwefel, H.E. Tureci, A.D. Stone, and R.K. Chang, "Progress in asymmetric resonant cavities: using shape as a design parameter in dielectric microcavity lasers," In: Optical Microcavities, Ed. K. Vahala, World Scientific, Singapore, 415–496 (2004).
7. A.I. Nosich, E.I. Smotrova, S.V. Boriskina, T.M. Benson, and P. Sewell, "Trends in microdisk laser research and linear optical modeling," Opt. Quant. Electronics, **39** (15), 1253-1272 (2007).
8. T. Harayama and S. Shinohara, "Two-dimensional microcavity lasers," Laser Photonics Rev., **5** (2), 247-281 (2011).
9. W. Poon, F. Courvoisier, and R. K. Chang, "Multimode resonances in square-shaped optical microcavities," Opt. Letts., **26** (9), 632-634 (2001).
10. J. Wiersig, "Hexagonal dielectric resonators and microcrystal lasers," Phys. Rev. A, **67**, 023807 (2003).
11. S.-K. Kim, S.-H. Kim, G.-H., Kim, H.-G. Park, D.-J. Shin, and Y.-H. Lee, "Highly directional emission from few-micron-size elliptical microdisks," Appl. Phys. Lett., **84** (6), 861–863 (2004).
12. C.-M. Lai, H.-M. Wu, P.-C. Huang, S.-L. Wang, and L.-H. Peng, "Single mode stimulated emission from prismlike gallium nitride submicron cavity," Appl. Phys. Letts., **90** (14), 1106-1108 (2007).
13. S R. Dubertrand, E. Bogomolny, N. Djellali, M. Lebental, and C. Schmit, "Circular dielectric cavity and its deformations," Phys. Rev. A., **77**(1), 013804(16) (2008).
14. S.V. Boriskina, T.M. Benson, P. Sewell, and A.I. Nosich, "Q-factor and emission pattern control of the whispering gallery modes in notched microdisk resonators," IEEE J. Selected Topics Quantum Electronics, **12** (1), 66–70 (2006).
15. Q.J. Wang, C. Yan, N. Yu, J. Unterhinninghofen, J. Wiersig, C. Pflügl, L. Diehl, T. Edamura, M. Yamanishi, H. Kan, and F. Capasso, "Whispering-gallery mode resonators for highly unidirectional laser action," Proc. Nat. Ac. Sci., **107** (52), 22407-22412 (2010).
16. M. Kneissl, M. Teepe, N. Miyashita, N.M. Johnson, G.D. Chern, and R.K. Chang, "Current-injection spiral shaped microcavity disk laser diodes with unidirectional emission," Appl. Phys. Lett., **84** (14), 2485–2487 (2004).
17. T. Ben-Massaoud and J. Zyss, "Unidirectional laser emission from polymer-based spiral microdisks," Appl. Phys. Lett., **86,** 241110 (2005).

18. J. Wiersig and M. Hentschel, “Asymmetric scattering and nonorthogonal mode patterns in optical microspirals”, Phys. Rev. A, 73, 031802 (2006).
19. M. Hentschel, T.-Y. Kwon, M.A. Belkin, R. Audet, and F. Capasso, “Angular emission characteristics of quantum cascade spiral microlasers,” Opt. Express, **17** (12), 10335-10343 (2009).
20. E.I. Smotrova, T.M. Benson, J. Ctyroky, R. Sauleau, and A.I. Nosich, “Optical fields of the lowest modes in a uniformly active thin sub-wavelength spiral microcavity,” Opt. Lett., **34** (24), 3773-3775 (2009).
21. J. Wiersig and M. Hentschel, “Combining directional light output and ultralow loss in deformed microdisks,” Phys. Rev. Lett., **100**, 033901, 2008.
22. Q. Song, W. Fang, B. Liu, S.-T. Ho, G.S. Solomon, and H. Cao, “Chaotic microcavity laser with high quality factor and unidirectional output,” Phys. Rev. A, **80**, 041807(R) (2009).
23. Q.H. Song, L. Ge, A.D. Stone, H. Cao, J. Wiersig, J.-B. Shin, J. Unterhinninghofen, W. Fang, and G.S. Solomon, “Directional laser emission from a wavelength-scale chaotic microcavity,” Phys. Rev. Letts., **105**, 103902 (2010).
24. Q.H. Song, L. Ge, J. Wiersig, J.-B. Shim, J. Unterhinninghofen, A. Eberspacher, W. Fang, G. S. Solomon, and H. Cao, “Wavelength-scale deformed microdisk lasers,” Phys. Rev. A., **84**, 063843 (2011).
25. C. Muller, *Foundations of the Mathematical Theory of Electromagnetic Waves,* Springer, Berlin (1969).
26. S.V. Boriskina, T.M. Benson, P. Sewell, and A.I. Nosich, “Accurate simulation of 2-D optical microcavities with uniquely solvable boundary integral equations and trigonometric-Galerkin discretization,” J. Opt. Soc. Am. A, **21**(3), 393–402 (2004).
27. A.F. Peterson, “The ‘interior resonance’ problem associated with surface integral equations of electromagnetics: numerical consequences and a survey of remedies,” Electromagnetics, **10**,293–312 (1990).
28. V. Rokhlin, “Rapid solution of integral equations of scattering theory in two dimensions,” J. Comput. Phys., **86**, 414–439 (1990).
29. D. Colton, R. Kress, *Inverse Acoustic and Electromagnetic Scattering Theory*, Springer, Berlin (1998).
30. L. Wang, J.A. Cox, and A. Friedman, “Modal analysis of homogeneous optical waveguides by the boundary integral formulation and Nystrom method,” J. Opt. Soc. Am. A., **15** (1), 92–100 (1998).
31. E.I. Smotrova, V.O. Byelobrov, T.M. Benson, J. Ctyroky, R. Sauleau, and A.I. Nosich, "Optical theorem helps understand thresholds of lasing in microcavities with active regions," IEEE J. Quantum Electronics, **47** (1), 20-30 (2011).
32. J.L. Tsalamengas, “Exponentially converging Nystrom methods applied to the integral-integrodifferential equations of oblique scattering / hybrid mode propagation in presence of composite dielectric cylinders of arbitrary cross-section,” IEEE Trans. Antennas Propagat. **55** (11), 3239-3250 (2007).
33. Z.T. Nazarchuk, *Numerical Analysis of Wave Diffraction by Cylindrical Structures*, Naukova Dumka Publ., Kiev (1989) (in Russian).
34. Y.V. Gandel, *Introduction to the Methods of Computation of Singular and Hyper-Singular Integrals*, Kharkiv Nat. Univ. Press., Kharkiv (2001) (in Russian).
35. M. Abramowitz and I. Stegun, *Handbook of Mathematical Functions*, Nat. Bureau of Standards Publ. (1964).